

Article citation info:

Zhao Y, Reliability and Fire Performance of Built-up (Battened) Cold-formed Steel Columns: Numerical study, *Eksploracja i Niezawodność – Maintenance and Reliability* 2025: 27(2) <http://doi.org/10.17531/ein/195810>

## Reliability and Fire Performance of Built-up (Battened) Cold-formed Steel Columns: Numerical study

Indexed by:  


Yang Zhao<sup>a,\*</sup>

<sup>a</sup> College of Fire Protection Engineering, China People's Police University, China

### Highlights


- Enhancing fire resistance in cold-formed steel columns for structural safety.
- Utilizing ABAQUS to study steel thickness, grade, and cross-sectional shapes.
- Thicker steel (1.95 mm) delays failure to 73.49 min, improving fire resistance.
- Grade 450 steel lasts 61.46 min, outperforming Grade 550 steel at 40.94 min.
- Effective design and materials crucial for better fire safety in CFS structures.

### Abstract

Cold-formed steel (CFS) columns play a crucial role in modern construction due to their lightweight, prefabricated, and recyclable characteristics, contributing significantly to structural safety and reliability. However, unprotected CFS columns lose their load-bearing capacity within 10-15 minutes under fire conditions. This study reviews recent advancements aimed at improving the fire resistance of CFS columns, focusing on factors such as steel thickness, grade, cross-sectional shape, and fire protection materials. Using ABAQUS software, validated against experimental data, parametric studies reveal that thicker sections and higher-grade steels enhance fire resistance, delaying structural failure. Fire protection strategies, such as plasterboard encasement, further bolster safety. The Complex cross-sectional shape demonstrated the highest load capacity (178.51 kN), while G450 steel outperformed other grades in both load capacity and fire resistance. Columns with 1.95 mm thickness provided the longest failure time (73.49 minutes).

### Keywords

battened column, built-up cold-formed steel column, numerical modeling, fire safety, nonlinear analysis, reliability

This is an open access article under the CC BY license (<https://creativecommons.org/licenses/by/4.0/>) 

### 1. Introduction

CFS columns serve as the main load-bearing elements in both single-story and multi-story CFS constructions; they play a critical role in ensuring building safety and reliability. CFS has several benefits, such as being lightweight, highly prefabricated, and recyclable. CFS constructions are widely used in several structures because of the material's exceptional strength-to-weight ratio, flexibility, and longevity. On the other hand, unplanned acts such as fire frequently result in severe property loss and, in the worst case, human casualties in buildings [1-3]. Thus, structural fire safety design and regular maintenance have drawn more attention during the past few decades. Previous fire studies conducted on unprotected CFS columns have

demonstrated their extreme vulnerability to elevated temperatures. These columns rapidly lose their ability to support loads within a short time frame of 10 to 15 minutes when exposed to fire [4-7]. Accordingly, investigations about fire loading in CFS columns are significant for ensuring their long-term reliability and safety. Then, Yin et al. in 2024, examined the performance of built-up columns made of CFS that are resistant to fire in mid-rise structures. According to this study, lowering the load ratio decreased the member's critical temperatures of the column, which in turn decreased fire resistance. Low heating rates and creep deformation significantly affected the resistance to fire. For non-uniform

(\*) Corresponding author.

E-mail addresses: Y. Zhao (ORCID: 0009-0004-6821-5726) [zhaoyang01@cpcu.edu.cn](mailto:zhaoyang01@cpcu.edu.cn)

specimens, temperature distribution patterns somewhat raised the members' critical temperatures [8]. For determining the critical buckling stress of CFS built-up columns with discrete fasteners, this research proposed a computational methodology by Yang et al. in 2023. The spline finite strip framework incorporates the fasteners' influence, represented as three-dimensional beam elements. The framework investigated how fasteners affect built-up sections' local, distortional, and global buckling modes. In comparison to unsheathed wall studs, the study demonstrates that encased wall panels prevent global buckling deformations [9-11]. Yang et al. in 2023, studied CFS built-up columns' fire resistance through tests and simulations. Screw spacing influences critical temperature and deformation modes, with composite action effectiveness shown at spacing < 300 mm [12]. Sam et al. 2023 examined the performance of two different CFS configurations, B-B and T-T, at different temperatures. Observations were made on the yield deformation and axial resistance. The CFS portions were simulated using ABAQUS [23] software, and the ultimate load of both the experiment and finite element model were compared, highlighting disparities in terms of percentage and ratio [13]. Pires et al. in 2021, examined ten fire resistance exams on steel columns made from CFS profiles, using load levels, thermal expansion restraint, and fire protection material. A numeric model simulates column behavior, showing that plasterboard hollow encasement significantly increases fire resistance, suggesting it is an alternative to built-up columns [14]. Through an experimental program that was done by Chen et al. in 2021, the residual material properties of CFS elliptical hollow sections (CFSEHS) were exposed to fire. Test specimens were subjected to a range of temperatures, heated in a gas furnace, and allowed to occur naturally. Stress-strain curves following the fire were used to assess residual material variables and characteristics [15]. Yang et al. in 2020, examined the box built-up columns made of CFS, resistant to fire in mid-rise structures. According to this study, lowering the load ratio decreased the member critical temperatures of the column, which decreased fire resistance. Low heating rates and creep deformation significantly affected the resistance to fire. For non-uniform specimens, temperature distribution patterns somewhat raised the members' critical temperatures [16]. Yang et al. in 2020, examined the fire resistance of CFS columns with built-up box-

shape sections using coupon tensile tests, load-bearing capacity tests, and parametric analyses. Results revealed global and local flexural buckling as the main failure mode [17]. Muftah et al. in 2018, investigated a CFS as a widely used material that offered benefits such as efficient manufacturing and straightforward assembly. Nevertheless, it encountered problems with buckling, particularly in elevated temperatures. This study discussed the fire resistance testing conducted on constructed box-shaped CFS columns [18]. Craveiro et al, in 2016, conducted an experimental study on compressed CFS columns with closed cross-sections and restrained thermal elongation, demonstrating that higher non-dimensional axial restraint ratio and column load levels resulted in lower critical temperatures. This suggested that the critical temperature limit specified in the EN 1993-1-3:2005 [19] code for fire design might be excessively cautious [20]. In 2015, Rodrigues conducted an investigational study on the fire behavior of compressed CFS columns, examining the effect of boundary conditions, loading level, and structural limitations. The study demonstrated that decreasing critical temperatures was achieved by increasing the column load levels and axial restraint ratio [21]. Abreu et al. in 2014, conducted experimental research on compressed CFS columns with closed cross-sections and restrained thermal elongation, revealing that increasing non-dimensional axial restraint ratio and column load levels decreased critical temperatures, and that the EN 1993-1-3:2005 [19] critical temperature limit might be too conservative for fire design [22]. Craveiro et al. in 2013, provided an overview of the most advanced research on fire-resistant CFS columns and compared the findings with the current body of literature. The experimental setup at the University of Coimbra was designed to evaluate the mechanical characteristics, and failure patterns, streamline calculation techniques, and generate data for future research [23].

Previous studies have primarily focused on built-up columns without batten plates, which lack the additional lateral support provided by battens. In this paper, we specifically investigate built-up columns with batten plates under fire loading conditions, aiming to evaluate how the inclusion of batten plates influences their fire resistance and structural behavior. This study provides a more comprehensive understanding of the performance of battened columns, which had not been extensively explored in earlier research. This research integrates

numerical simulations to provide a comprehensive understanding of the fire performance of the battened built-up CFS columns. This multi-faceted approach ensures that the findings are robust and applicable to real-world scenarios, ultimately enhancing the safety, reliability, and maintenance practices associated with these structures. The objective of this research is to examine the response of the battened built-up steel column under non-uniform fire loading conditions. It examines how factors such as non-uniform temperature distribution, steel grade, thickness, and cross-section shape impact the Fire Resistance Rating (FRR) of the columns. The thermal analysis will provide time-temperature profiles, while the structural analysis will assess the relationship between load ratio, failure time, and critical temperature under fire conditions. Additionally, the study focuses on comparing cross-sectional shapes, including Complex, Sigma, and Inclined, and evaluates how variations in steel grade and thickness affect fire resistance. By addressing these factors, the study aims to offer insights for designing safer, fire-resistant CFS structures.

## 2. Numerical modeling

### 2.1. General

The finite element software ABAQUS 22.1 [24] was utilized to model and simulate the behavior of built-up CFS battened columns. The simulation framework included a detailed representation of the column geometry and the nonlinear material characteristics of the cross-section [25,26]. Conducting FEA for buckling involves two primary analysis types: Eigenvalue analysis, load-displacement and nonlinear analysis. The finite element (FE) thermal models employed two distinct surface conditions to simulate fire exposure: a film condition and radiation to ambient. These conditions represented heat transfer through convection and radiation, respectively. A quadrilateral element (DC2D4) with four nodes was used, facilitating linear heat conduction or mass dispersion. Conversely, the 3D model utilized solid brick elements (DC3D4) with eight nodes, each with a single degree of freedom. In the 2D thermal analysis, the convective heat transfer coefficient was set at 16 W/m<sup>2</sup>°C for the fire exposure curves, and 25 W/m<sup>2</sup>°C for the ISO 834 [27] fire curve. Radiative heat flux was computed using a steel emissivity of 0.24 for furnace conditions, and 0.7 for other surfaces. In the 3D thermal analysis, a radiative

property factor of 0.9 was applied to both sides of the plasterboard, regardless of fire exposure. The surface film coefficients were designated as 25 W/m<sup>2</sup>°C for fire-exposed surfaces and 10 W/m<sup>2</sup>°C for surfaces under normal conditions. The Stefan-Boltzmann constant was set at  $5.67 \times 10^{-8}$  W/m<sup>2</sup> °C. The thermal properties of steel were derived from EN 1993-1-2 [19], while those for plasterboard were sourced from research by Dias et al. [28]. The structural analysis process began with an Eigenvalue analysis to identify potential buckling modes of the columns. This analysis step involved applying the load and evaluating multiple buckling modes, with the most relevant mode predicted by the Eigenvalue analysis selected for further examination. This step is crucial as it determines the critical buckling modes under the given loading conditions, thus providing the basis for the subsequent detailed analysis. Following the Eigenvalue analysis, a load-displacement nonlinear analysis with static general step was performed at ambient temperature to obtain the ultimate compression capacity of the battened column. The validation process revealed that the static general method provided greater accuracy than the experimental data, leading to a better convergence of the numerical model. Subsequently, a nonlinear analysis of the column subjected to fire loading was conducted, considering a specific load ratio. This advanced analysis accounted for initial geometric imperfections and material nonlinearities, which are essential for realistic simulation. The outcomes of this analysis included the determination of ultimate load capacities, failure modes, failure time under fire conditions, and axial shortenings. This step identifies the primary buckling mode, which is the mode most likely to occur under the applied load. The identified mode then informs the nonlinear analysis, ensuring a realistic simulation of the column's structural behavior. The load-displacement nonlinear analysis goes beyond the linear assumptions of the Eigenvalue analysis by incorporating actual material and geometric nonlinearities, including initial imperfections. This comprehensive analysis provides a more accurate prediction of the column's response under fire condition. It determines the ultimate load-carrying capacity, failure times and specific failure modes, offering a detailed insight into the column's performance. These insights are essential for the engineering design and evaluation of such columns, ensuring their safety, reliability, and effective

application in structural engineering practices.

## 2.2. Mesh size and element type

In the model, CFS channels and batten plates were defined using the S4R shell element from the ABAQUS element library [23]. This shell element, which provides six degrees of freedom per node, was selected due to its ability to deliver accurate solutions

across a wide range of applications. To achieve a balance between accuracy and computational efficiency in modeling the CFS built-up section the columns, convergence studies were performed. These studies determined that a fine mesh size of  $5 \times 5$  mm (length  $\times$  width) was optimal, providing a reasonable level of accuracy, as illustrated in Fig. 1.

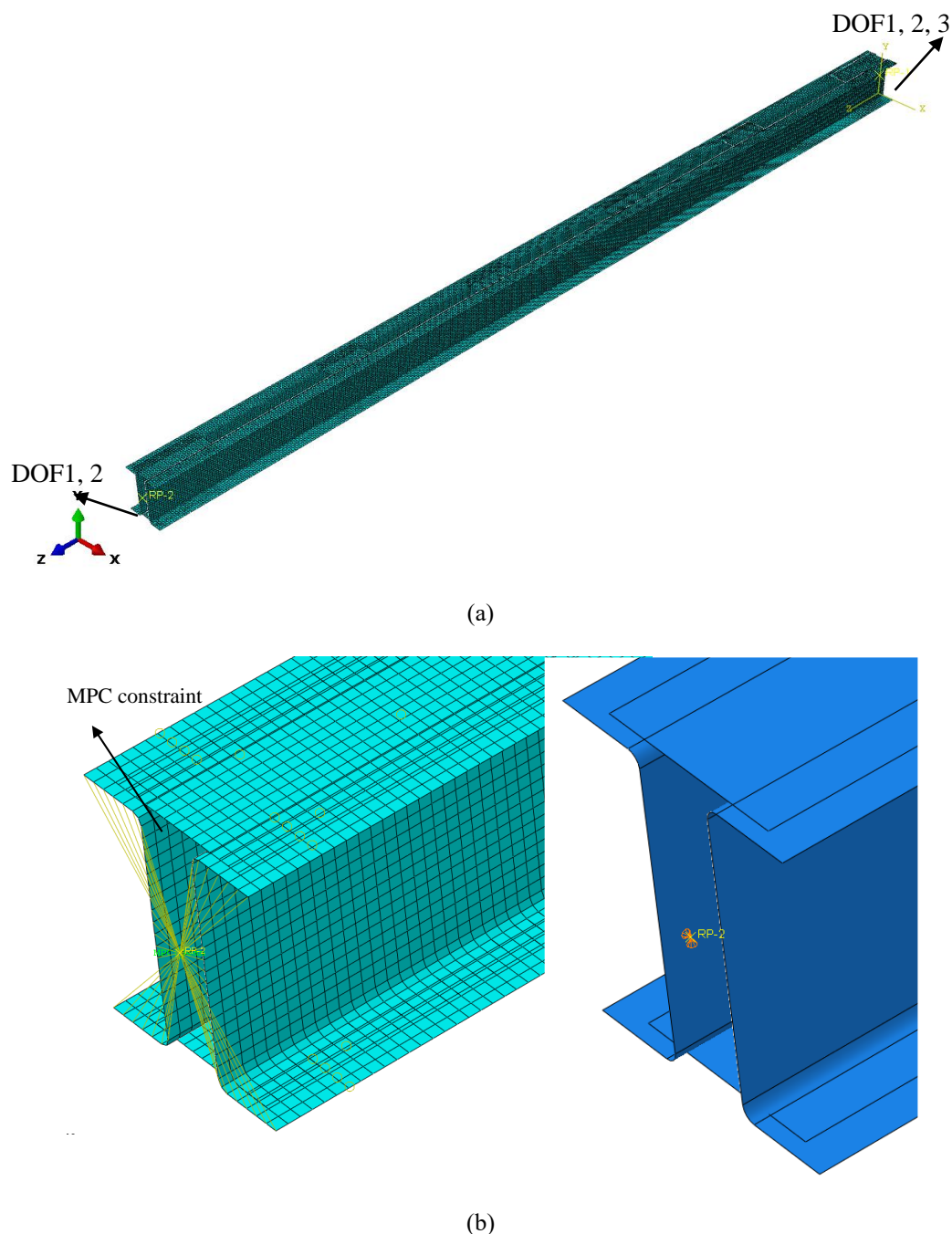


Fig. 1. Numerical model of built-up batted column.

## 2.3. Material modelling

The measured stress-strain curves for the flat portions of the channels [29] were integrated into the finite element models.

The elastic-plastic material model provided in ABAQUS, [25] enabling the use of a nonlinear stress-strain curve. The initial portion of this curve characterizes the elastic response, up to the proportional limit stress, defined by the measured Young's

modulus ( $E_0$ ). Within the elastic region, the Poisson's ratio was set at 0.3. Given that post-buckling analysis involves significant inelastic strains, the nominal (engineering) static stress-strain curve was converted into a true stress and logarithmic plastic strain curve. The true stress ( $\sigma_{true}$ ) and plastic true strain ( $\sigma_{ln}^{pl}$ ) required by ABAQUS [23] were computed using Eqs. (1) and (2).

$$\sigma_{true} = \sigma_{nom}(1 + \varepsilon_{norm}) \quad 1(a)$$

$$\varepsilon_{ln}^{pl} = \ln(1 + \varepsilon_{norm}) - \frac{\sigma_{true}}{E} \quad 1(b)$$

## 2.4. Boundary condition

The built-up CFS section battened columns examined in this study were designed as pin-ended columns. Boundary conditions were applied to the independent node of the rigid Multi-Point Constraint (MPC) at both the lower and upper ends of the model, with dependent nodes connected to these independent nodes via beam elements, as depicted in Fig. 1(b). To replicate simply supported end conditions, constraints were imposed on movements along the Y, X, and Z axes at the lower sections of the studs. Similarly, the upper part of the stud was restricted in translations along the Y and X axes. DOF (degree of freedom) 1, 2, and 3 correspond to the x, y, and z axes in ABAQUS [25]. Loading was applied incrementally to the reference point (RP) at the upper end of the column using the modified STATIC GENERAL method available in the ABAQUS [25] library. This method accounts for geometric and material nonlinearities, providing a more accurate simulation of the column's behavior under load. The STATIC GENERAL method is particularly effective in tracing the post-buckling response, capturing both pre- and post-buckling behaviors of the columns. To impose the fire load, a transient state method was employed. Initially, a fraction of the ultimate compressive load at room temperature was applied to the column. Subsequently, the time-temperature curve derived from thermal analysis was applied, continuing until column failure occurred. The batten plates were constrained to the CFS channels using a "Tie" constraint to ensure consistent displacements and rotations throughout the loading process. Tie constraint in ABAQUS [23] facilitates the automatic coupling of three-dimensional shell meshes, ensuring a unified displacement and rotation response under loading.

## 2.5. Initial imperfection

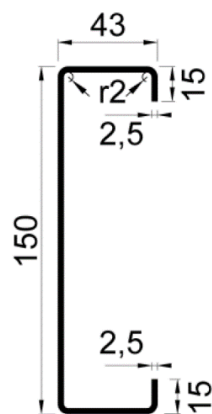
Both initial local and overall geometric imperfections are typically present in columns due to fabrication and transportation processes. Accurate FEA therefore necessitates the superposition of local and overall buckling modes, each scaled by their measured magnitudes. Local buckling modes reflect the inherent imperfections in the column's sections, while global buckling modes capture the imperfections along the entire column length. To accurately capture these effects, buckling modes should be derived from an Eigenvalue analysis of the column with varying thicknesses: a very small thickness to provoke local buckling, and a very large thickness to induce global buckling. For the columns tested in this study, the average measured global imperfections were approximately 1/1100 of the specimen length [30-32]. Local imperfections were taken as 0.5% of the channel thickness, consistent with recommendations in [33]. By incorporating these measured imperfection magnitudes into the buckling modes, the FEA can more precisely simulate the column's actual behavior under load, providing critical insights into its structural performance. This methodology underscores the importance of accurately modeling imperfections for reliable FEA results, particularly for predicting buckling and post-buckling responses in built-up CFS columns under fire condition.

## 3. Validation of numerical results

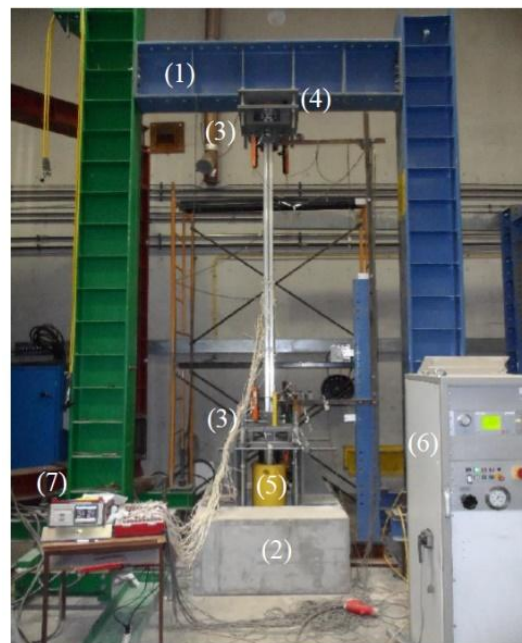
To validate the structural and thermal models, this study leveraged previous research by Craveiro et al. (2014) [24] and the numerical model developed by Senthilkumar et al. (2021) [34]. The validation focused on CFS columns subjected to fire conditions, as tested at the University of Coimbra in Portugal. The experiments specifically investigated lipped channel columns constrained against thermal expansion, with an axial stiffness of 3 kN/m (Fig.2). The column cross-section details are shown in Fig. 2(a), with C-shaped columns featuring a cross-section of 150 mm in height, 43 mm in width, and 2.5 mm in thickness, and an overall length of 2950 mm. In the experimental setup (Fig. 2(b)), the service load was regulated via a load cell placed between the upper beams of the restraining structure and a hydraulic jack, maintaining a constant initial load throughout the test. A vertical modular electric furnace, designed to follow the standard fire curve ISO 834 (1999), was

utilized to apply thermal effects. As the CFS column was heated, thermal expansion led to elongation, but due to the column's restraint, additional axial forces developed. This comprehensive experimental setup is depicted in Fig. 2. The validation process for the thermal and structural finite element models involved several steps. Initially, the thermal model's credibility was established by comparing the results of a 2D thermal analysis with the time-temperature profiles obtained from empirical and numerical studies conducted by Craveiro et al. [29]. The strong correlation observed, as shown in Fig. 3, substantiates the thermal model's accuracy in replicating the experimental thermal behavior. Subsequently, the structural model was validated under both ambient and elevated temperatures. The model's performance under axial compression until collapse at room temperature was compared with existing experimental and computational data. This comparison, illustrated in Fig. 4, demonstrated the alignment of axial compressive forces with the column's axial response, confirming the structural model's accuracy at ambient conditions. Furthermore, Fig. 5 compares the experimental results with finite element method (FEM) outputs in terms of axial force versus axial displacement, axial displacement versus temperature, and the ratio of axial force to

initial load ( $R/P_i$ ) versus temperature. The close agreement between the FEM predictions and the empirical and numerical results further verifies the structural model's precision across various conditions. This includes the model's ability to capture complex interactions between thermal expansion and mechanical restraint under fire exposure. Overall, this thorough validation process ensures the reliability of both the thermal and structural finite element models. The models are demonstrated to be robust in predicting the behavior of CFS columns under different loading and thermal scenarios, enhancing confidence in their application for assessing the structural integrity and fire performance of such columns. Fig. 6 compares the buckling modes of the column after fire loading with the failure modes observed in the experimental results. This comparison strengthens the credibility of the numerical analysis in accurately simulating the behavior of CFS columns under fire conditions, accounting for the restraint due to thermal elongation. Both the experimental findings and finite element simulations successfully identified flexural instability around the minor axis of the CFS columns, as well as the presence of local and distortional buckling patterns.

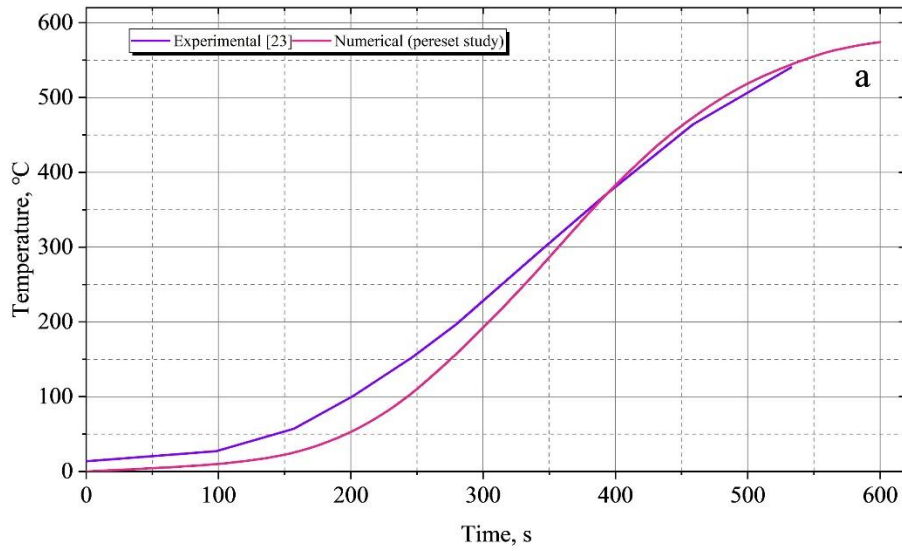


(a)



(b)

Fig. 2. Experimental set up: (a) overall view of column (b) column cross section shape in mm [29].



(a)



(b)

Fig. 3. Verification of heat transfer analysis.

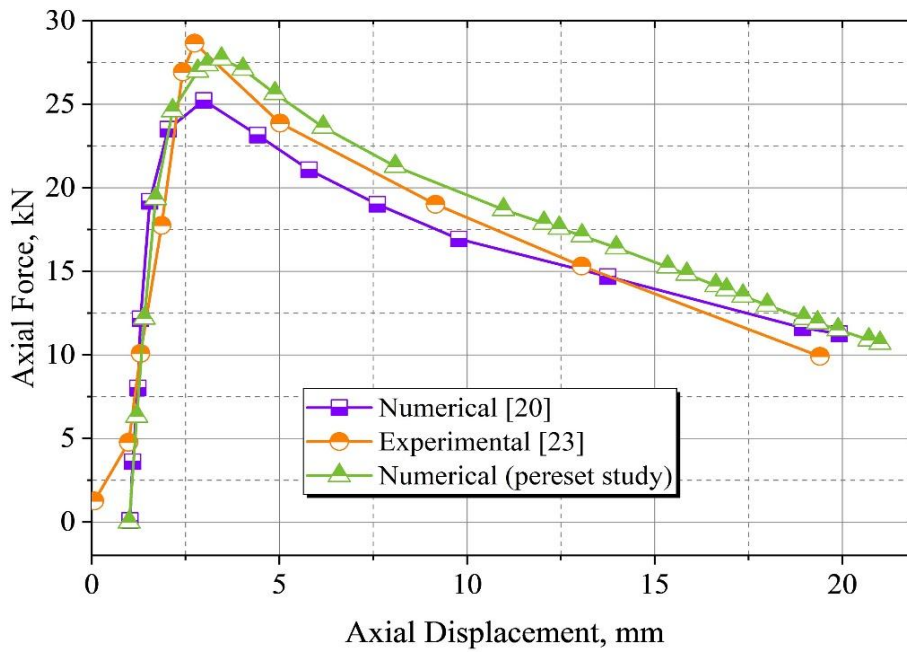


Fig. 4. Verification structural model at ambient temperature.



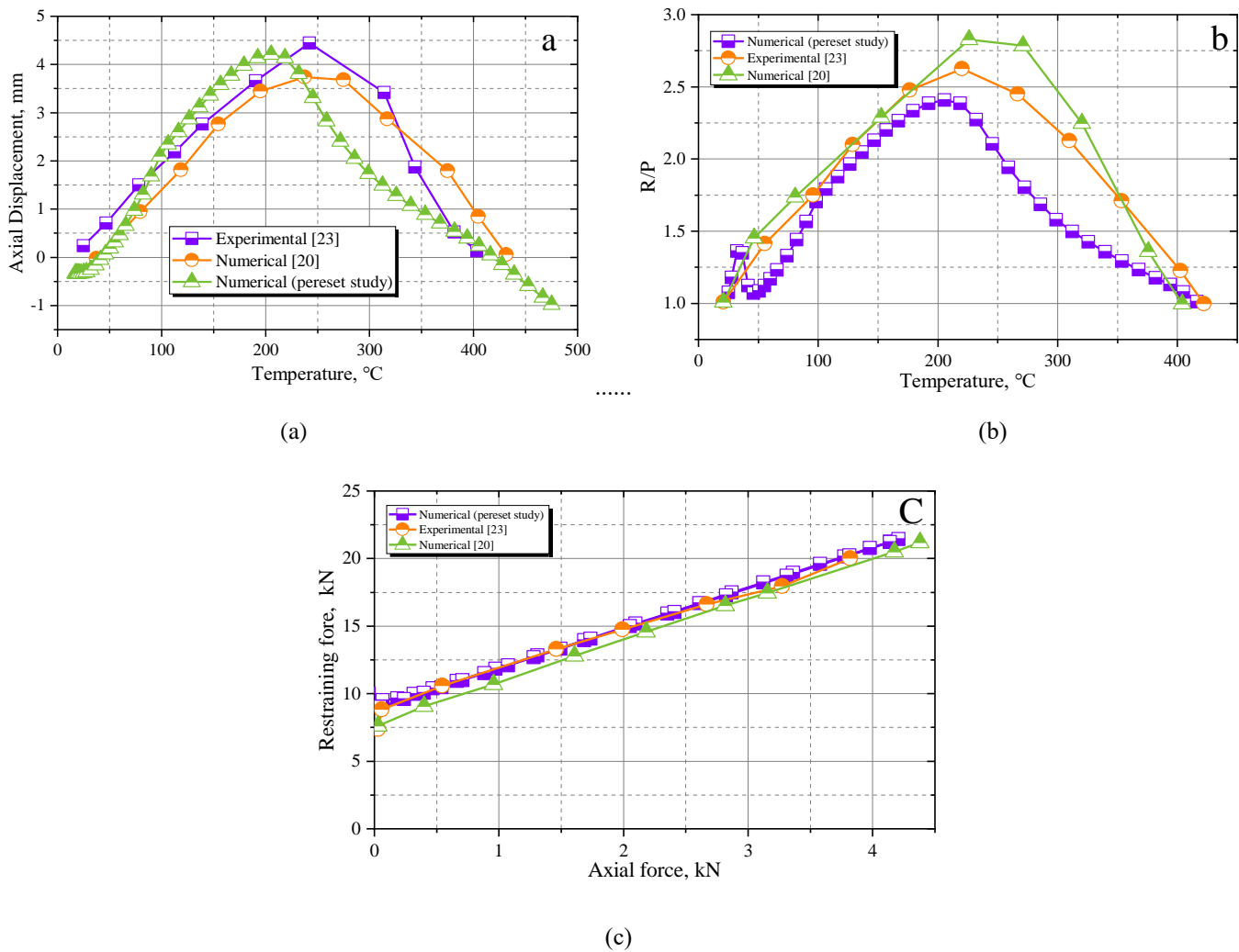


Fig. 5. Comparison between the experimental and finite element method outputs.

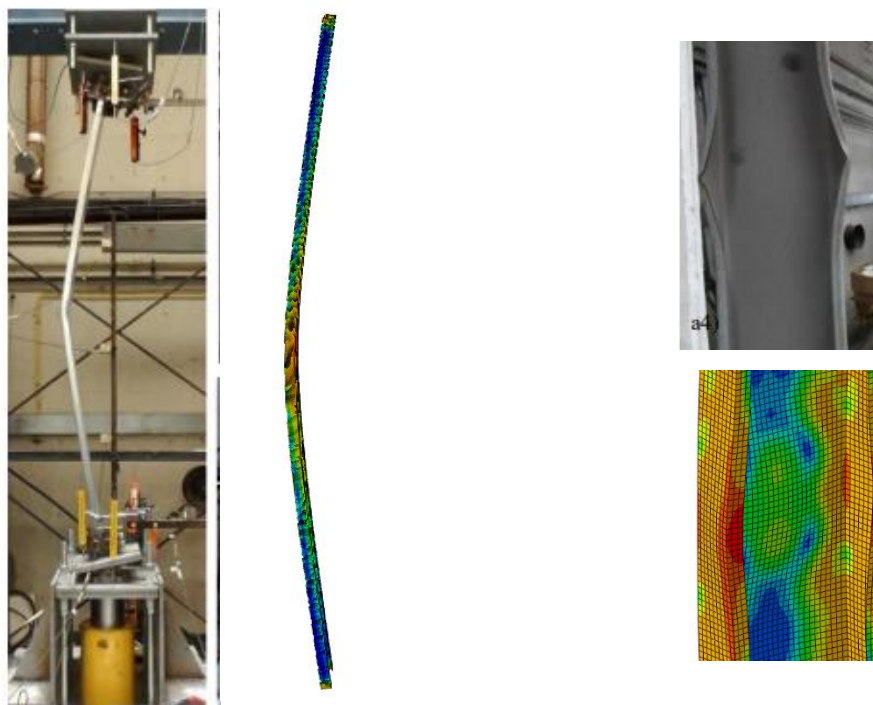


Fig. 6. comparison between failure modes of the column under fire.



#### 4. Parametric Study

In this study, a comprehensive parametric analysis was conducted to evaluate the performance of built-up (battened) CFS columns under fire conditions. The analysis considered variations in column cross-section shapes (Inclined, Complex, C-shaped, and Sigma), steel grades (G250, G450, and G550), and steel thicknesses (0.6 mm, 0.95 mm, 1.55 mm, and 1.95 mm). This shape provides enhanced stability against lateral torsional buckling but might be more complex in terms of fabrication. The cross-section shape of CFS columns is a critical factor influencing their structural performance. Different shapes exhibit varying degrees of susceptibility to buckling, load-bearing capacity, and thermal response. Complex shapes can optimize strength and stiffness, often used in specialized applications where both axial and lateral loads are significant. A common cross-section in CFS design, C-shaped columns balance ease of manufacturing with reasonable structural performance. Sigma shapes offer improved resistance to local buckling and can be advantageous in high-load scenarios due to their inherent geometric stability. Understanding the performance variations among these cross-sections under fire conditions helps in selecting the most effective design for specific applications, ensuring safety and reliability. The steel grade defines the material's strength and ductility. Analyzing different steel grades under fire conditions is crucial to understanding how material strength and ductility impact the column's structural integrity and failure behavior during fire exposure. Steel thickness affects the column's overall stiffness, load capacity, and thermal resistance. Evaluating varying thicknesses allows for an assessment of how structural and thermal performance evolves with changes in material dimensions, informing optimal design choices for fire-resistant structures. The key outputs from the parametric study were: **Load-Axial Shortening at Ambient Temperature:** This output captures the relationship between applied loads and the resulting axial shortening of the columns at room temperature. It provides insights into the elastic and plastic deformation characteristics of the columns, crucial for understanding their performance under normal service conditions. **Load-Failure Time at Elevated Temperature:** This output measures the time until failure when the columns are exposed to elevated

temperatures while under a load. It reflects the fire resistance of the columns, including their ability to sustain structural integrity under fire exposure. By systematically varying the cross-section shape, steel grade, and thickness, the study elucidates how each parameter influences the structural and thermal performance of built-up CFS columns. These insights are essential for designing columns that meet specific performance criteria under both ambient and fire conditions, ultimately contributing to safer and more efficient structural designs in fire-prone environments. To generate a strain-stress curve at elevated temperatures, we applied the reduction factors for modulus of elasticity and yield strength as recommended by Kankanage and Mahendran [35] for CFS grades t1.9-G450, t1.5-G450, t1.95-G250, and t1.55-G250. For the CFS grades t0.95-G550, t0.6-G550, t0.95-G250, and t0.6-G250, we utilized the reduction factors derived from the research conducted by Ranawaka and Mahendran [36].

##### 4.1. Thermal analysis results

Fig. 7 presents a comprehensive analysis of how variations in steel thickness influence the temperature distribution across different cross-sectional shapes of columns. Specifically, it reveals that increasing the thickness of steel significantly decreases the temperature of the hot flange. At the 40-minute mark, the maximum reduction in hot flange temperature is observed to be 210°C for complex sections, 245°C for inclined sections, 192°C for C sections, and 244°C for sigma sections. Examining Fig.7, the most substantial decrease in cold flange temperature is recorded at 118 minutes with an increase in thickness from 0.6 mm to 1.95 mm. The cold flange temperature increases for complex, inclined, C, and sigma columns at this time point is 42°C, 101°C, 62°C, and 67°C, respectively. This data underscores the significant impact of steel thickness on the thermal behavior of the cold flange, especially over extended exposure periods. In the web section, the temperature response mirrors that of the hot flange, where an increase in thickness correlates with a decrease in web temperature across various cross-sectional shapes. However, the temperature variations in the web are less pronounced than those observed in the hot and cold flanges. At 50 minutes, the maximum temperature reduction in the web is 106°C for complex sections, 100°C for inclined sections, 96°C for C sections, and 97°C for sigma-shaped sections. These findings suggest that while steel

thickness is a crucial factor, the effect on web temperature is somewhat moderated compared to the flanges. Fig. 7 further illustrates the temperature changes in the web of the steel columns, highlighting that for different cross-sectional shapes and steel thicknesses, the temperature variation is nearly linear. This consistency suggests that the cross-sectional shape exerts a negligible influence on the temperature distribution within the web section, maintaining a uniform profile over time. Overall,

the data indicates that increasing the thickness of steel significantly impacts the thermal performance of column sections, primarily by reducing temperatures in the hot flange and web. Although different cross-sectional shapes are considered, their effect on the temperature distribution is minimal, with temperature-time profiles for the web, hot, and cold flanges showing considerable uniformity across various shapes.

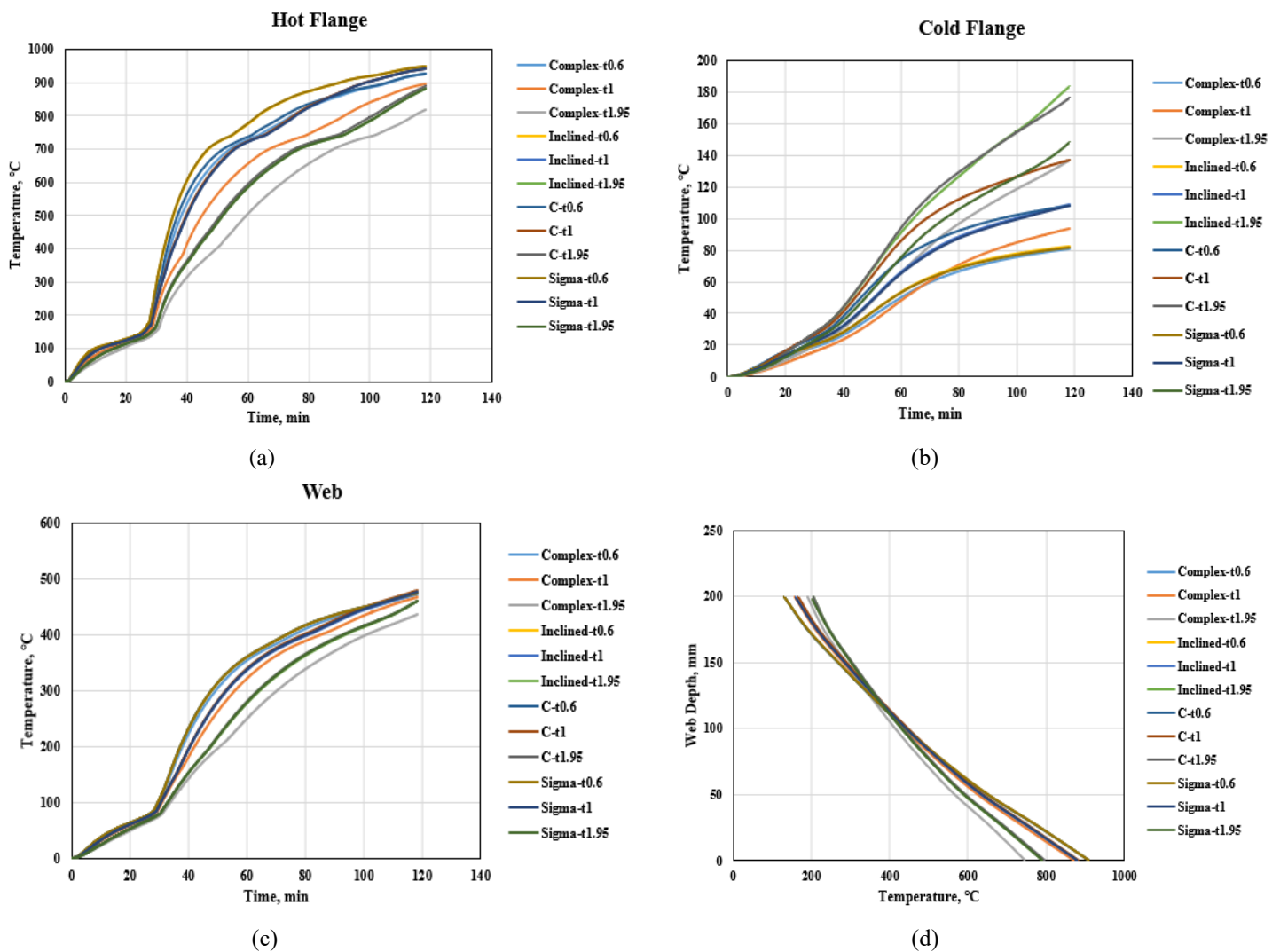


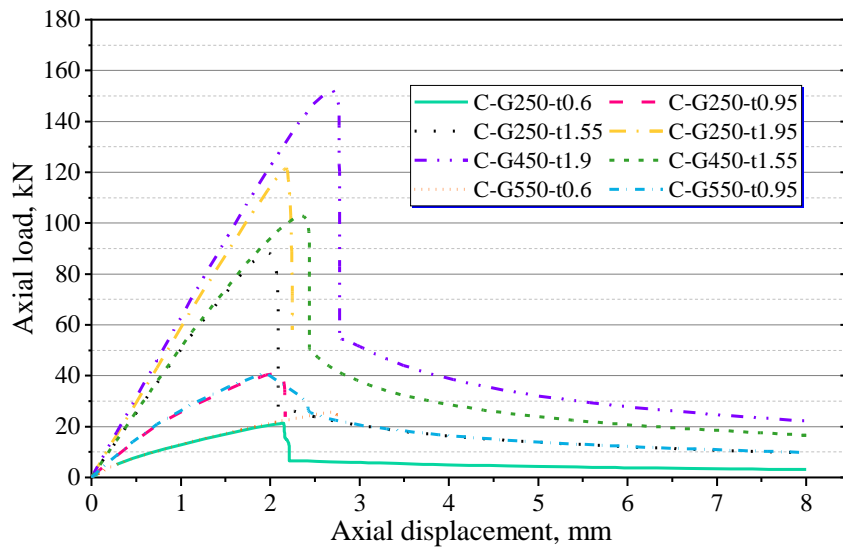
Fig. 7. Heat transfer analysis results.

## 4.2. Nonlinear analysis results

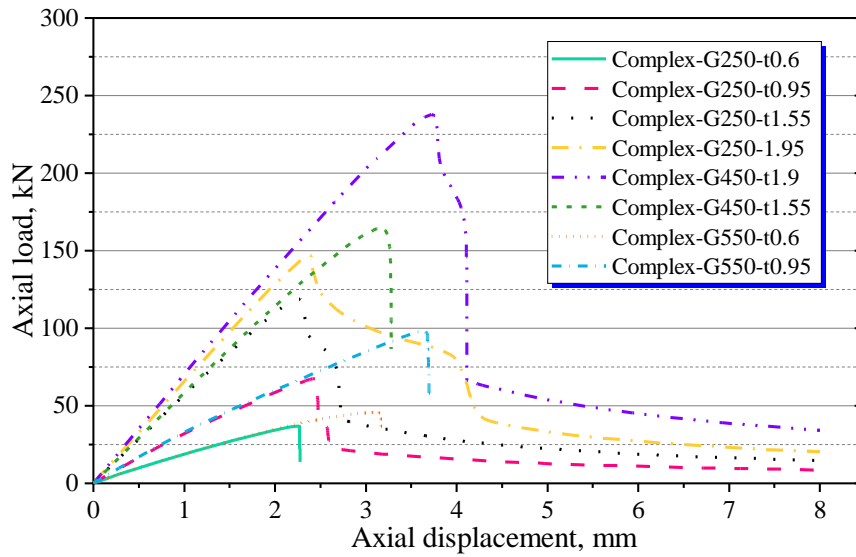
### 4.2.1. Nonlinear evaluation results at room temperature

The results of the structural analysis at ambient temperature are presented as axial load versus axial displacement diagrams. Initially, the effects of column section dimensions, steel

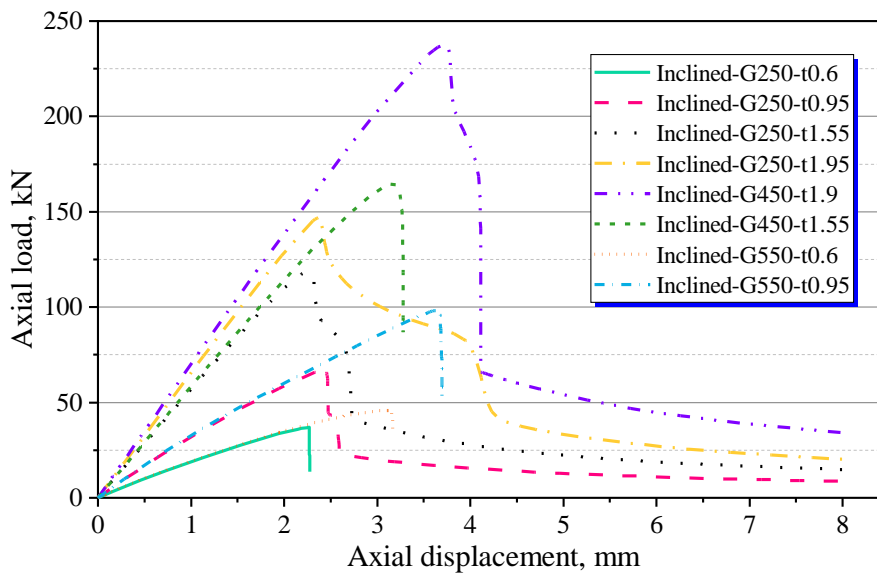
thickness, and steel type on the ultimate capacity of the composite column at room temperature were examined. Subsequently, the failure time of the column under fire conditions was analyzed. Fig. 8 shows the axial load-axial shortening of columns at ambient temperature.



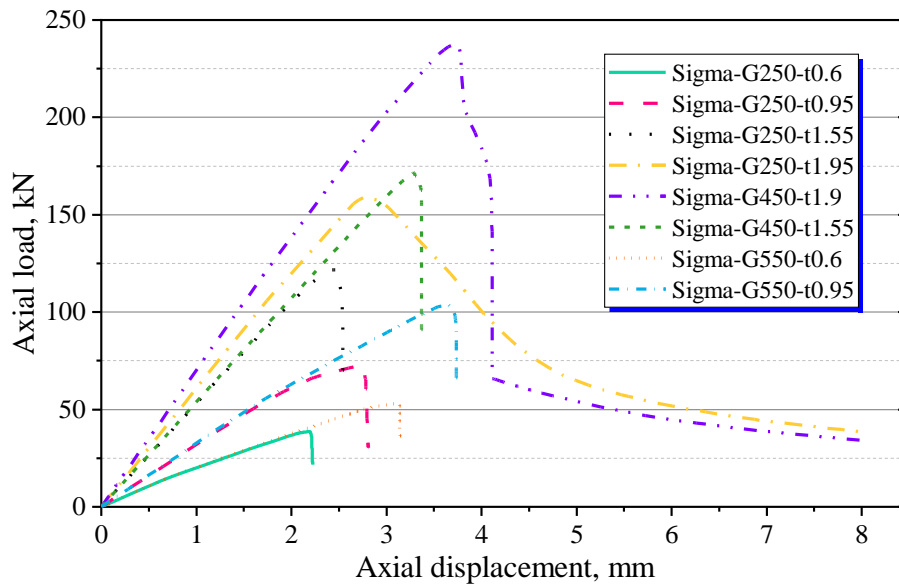
(a)



(b)



(c)



(d)

Fig. 8. Nonlinear analysis results at ambient temperature.

#### 4.2.1.1. Effect of Column Cross-Section Shape on Ultimate Load

Table 1 presents a summary of the analysis of ultimate load variations for different column cross-section shapes. As illustrated in Fig. 9, the C-shaped column exhibits the lowest average ultimate load at 74.31 kN, indicating a comparatively lower load-bearing capacity. In contrast, the Complex shape demonstrates a significantly higher average ultimate load of 178.51 kN, representing a 140.23% increase over the C shape, highlighting its superior load-bearing performance. The Inclined shape, with an average ultimate load of 97.03 kN, shows a 45.64% reduction compared to the Complex shape, indicating that while it performs better than the C shape, it is less effective than the Complex shape. The Sigma-shaped column, with an average ultimate load of 119.77 kN, displays a 23.44% increase compared to the Inclined shape, demonstrating improved load-bearing capacity. Additionally, an outlier value of 237.68 kN was observed for the Inclined shape, though it is based on a single data point and requires further validation. Overall, the cross-sectional shape has a pronounced effect on the ultimate load capacity, with the Complex shape offering the best performance, followed by the Sigma, Inclined, and C shapes. These findings underscore the importance of cross-sectional design in optimizing the structural performance of columns.

Table 1. Ultimate load variations for different column cross-section shapes.

Shape	Mean	std	Count	pct_difference
C	74.31	48.83	8	
Complex	178.51	61.5	8	140.23
Inclined	97.03	49.41	7	-45.64
Sigma	119.77	67.2	8	23.44
Inclined	237.68		1	98.45

**Mean:** The average load-bearing capacity (in kN or other relevant units) measured during the tests for each shape.

**Std.:** The standard deviation of the load-bearing capacity, indicating the variability of the test results for each shape.

**Count:** The number of samples tested for each shape.

**pct\_difference:** The percentage difference in load-bearing capacity compared to the baseline shape (C-shape), reflecting the performance increase or decrease of each shape.

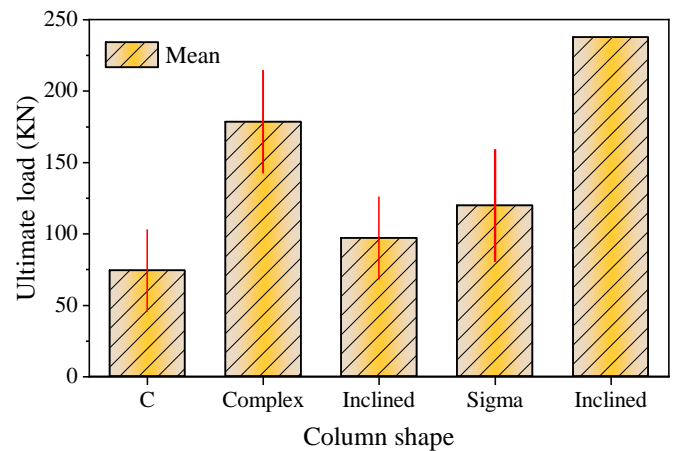


Fig. 9. Ultimate load variations for different column cross-section shapes.

#### 4.2.1.2. Effect of Steel Grade on Ultimate Load

Fig. 10 and Table 2 show the effect of steel grade on the ultimate load of column at ambient temperature.

Table 2. Ultimate load variations for different steel grades.

Grade	Mean	std	Count	pct_difference
G250	99.55	49.85	16	
G450	195.01	56.58	8	95.89
G550	93.09	69.55	8	-52.27

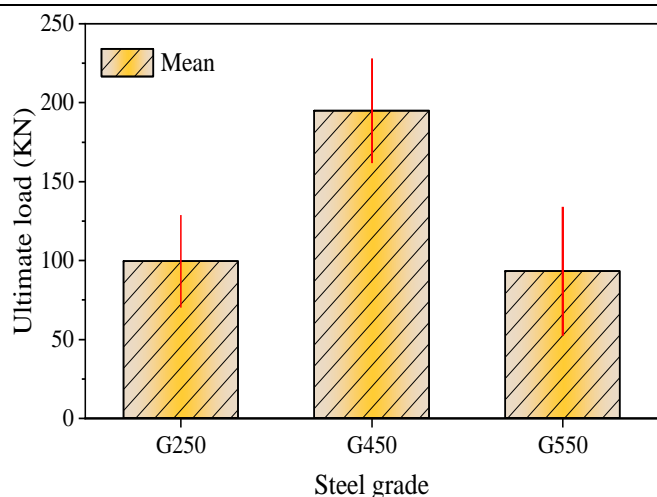


Fig. 10. Effect of Steel Grade on Ultimate Load.

G250 Steel Grade exhibits an average ultimate load of 99.55 kN. This serves as the baseline for comparison with other grades. G450 Steel Grade shows a significantly higher average ultimate load of 195.01 kN, representing a 95.89% increase compared to G250. This substantial improvement indicates that the G450 steel grade provides a much better load-bearing capacity. The average ultimate load for G550 Steel Grade decreases to 93.09 kN, which is a 52.27% reduction from the G450 grade. Despite being a higher grade, G550 demonstrates lower ultimate load capacity, possibly due to factors such as increased brittleness. The steel grade has a significant impact on the ultimate load capacity of columns. The G450 grade offers the best performance among the grades analyzed, significantly outperforming both G250 and G550. These results highlight the importance of selecting an appropriate steel grade for optimal load-bearing performance in structural applications.

#### 4.2.1.3. Effect of Steel thickness on Ultimate Load

Fig. 11 and table 3 indicate the average ultimate load for each steel thickness. 0.60 mm thickness steel exhibits an average ultimate load of 76.57 kN, serving as the baseline for comparison. 0.95 mm thickness steel shows a slight increase in

average ultimate load to 81.23 kN, representing a 6.09% increase compared to 0.60 mm. This indicates a minor improvement in load-bearing capacity. For 1.55 mm thickness steel the average ultimate load increases significantly to 149.27 kN, an 83.75% increase from 0.95 mm. This substantial improvement highlights the positive impact of increased thickness on load-bearing capacity. 1.90 mm Thickness steel exhibits the highest average ultimate load at 209.15 kN, which is a 40.12% increase compared to 1.55 mm. This indicates that increasing the thickness further enhances the load-bearing capacity significantly. 1.95 mm thickness steel shows a slight decrease in average ultimate load to 151.11 kN, a 27.75% reduction compared to 1.90 mm. This suggests that beyond a certain point, further increase in thickness may not contribute to an increase in load capacity and might even reduce it. The steel thickness has a significant impact on the ultimate load capacity of columns. The load-bearing capacity generally increases with increasing thickness, reaching a peak at 1.90 mm. However, the slight decrease at 1.95 mm indicates that there might be an optimal thickness for maximum load capacity. Table 4 shows the ultimate load that were obtained from nonlinear analysis of column at ambient temperature.

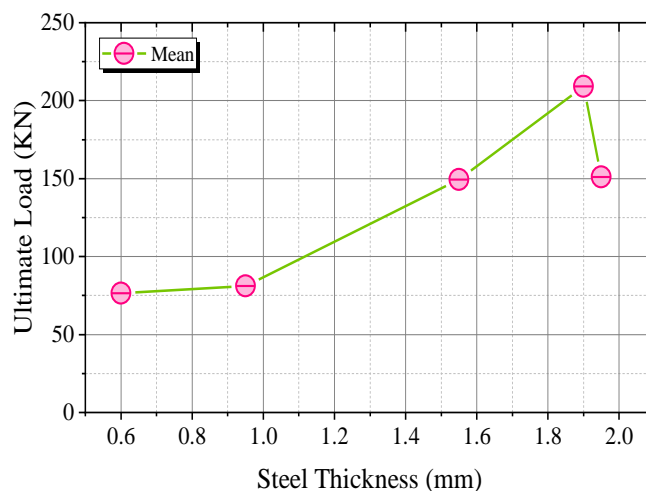


Fig. 1. Effect of Steel thickness on Ultimate Load.

Table 3. ultimate load variations for different steel thicknesses.

Thickness_mm	Mean	std	Count	pct_difference
0.6	76.57	77.19	8	
0.95	81.23	33.5	8	6.09
1.55	149.27	54.04	8	83.75
1.9	209.15	57.17	4	40.12
1.95	151.11	23.22	4	-27.75

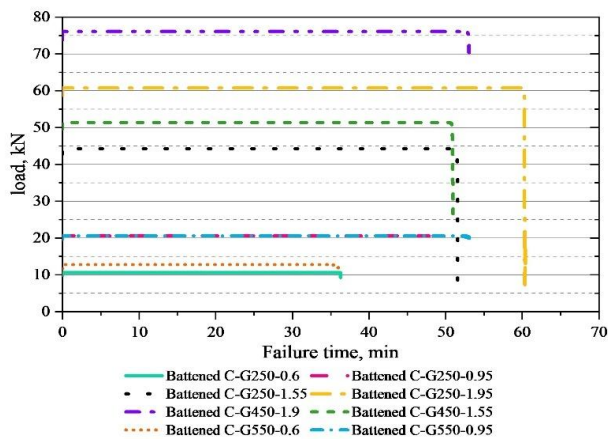
Table 4. Ultimate load of column at ambient temperature.

Column	Ultimate Load (kN)	Shape	Grade	Thickness (mm)
battened C-G250-0.6	21.2873	C	G250	0.6
battened C-G250-0.95	41.198	C	G250	0.95
battened C-G250-1.55	88.5308	C	G250	1.55
battened C-G250-1.95	121.51	C	G250	1.95
battened C-G450-1.9	152.292	C	G450	1.9
battened C-G450-1.55	102.762	C	G450	1.55
battened C-G550-0.6	25.6073	C	G550	0.6
battened C-G550-0.95	41.2858	C	G550	0.95
battened Complex-G250-0.6	155.534	Complex	G250	0.6
battened Complex-G250-0.95	83.6347	Complex	G250	0.95
battened Complex-G250-1.55	141.6	Complex	G250	1.55
battened Complex-G250-1.95	176.892	Complex	G250	1.95
battened Complex-G450-1.9	275.064	Complex	G450	1.9
battened Complex-G450-1.55	218.485	Complex	G450	1.55
battened Complex-G550-0.6	235.672	Complex	G550	0.6
battened Complex-G550-0.95	141.209	Complex	G550	0.95
Battened Inclined-G250-0.6	36.9558	Inclined	G250	0.6
Battened Inclined-G250-0.95	67.6244	Inclined	G250	0.95
Battened Inclined-G250-1.55	118.785	Inclined	G250	1.55
Battened Inclined-G250-1.95	147.165	Inclined	G250	1.95
battened inclined-G450-1.9	237.684	inclined	G450	1.9
Battened Inclined-G450-1.55	164.575	Inclined	G450	1.55
Battened Inclined-G550-0.6	45.795	Inclined	G550	0.6
Battened Inclined-G550-0.95	98.3113	Inclined	G550	0.95
battened Sigma-G250-0.6	38.6528	Sigma	G250	0.6
battened Sigma-G250-0.95	72.8477	Sigma	G250	0.95
battened Sigma-G250-1.55	121.713	Sigma	G250	1.55
battened Sigma-G250-1.95	158.883	Sigma	G250	1.95
battened Sigma-G450-1.55	237.684	Sigma	G450	1.55
battened Sigma-G450-1.9	171.563	Sigma	G450	1.9
battened Sigma-G550-0.6	53.073	Sigma	G550	0.6
battened Sigma-G550-0.95	103.755	Sigma	G550	0.95

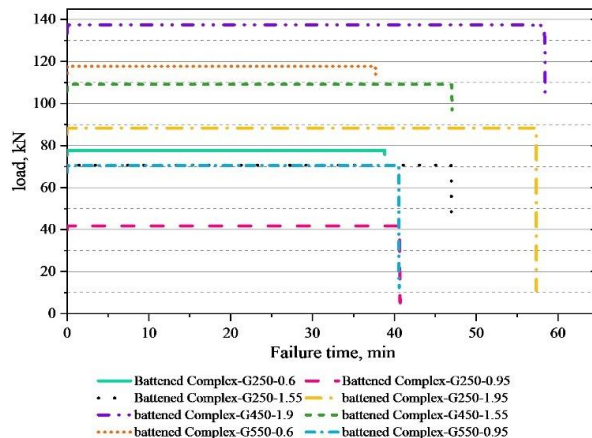
#### 4.2.2. Nonlinear evaluation results at elevated temperature

The nonlinear analysis results of columns at elevated temperature are in form of load-failure time. Fig. 12 shows the

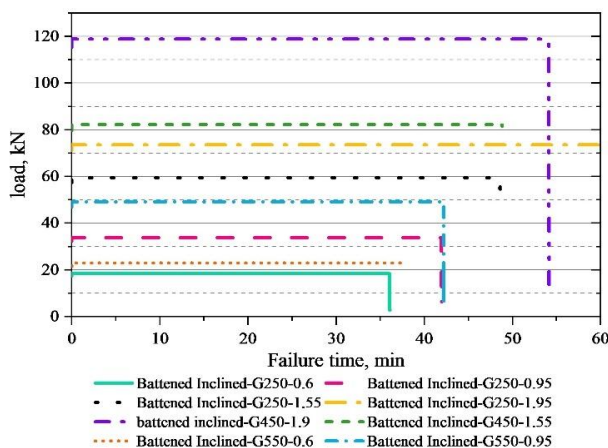
failure time of column at elevated temperature. In the next step, using the failure time obtained from these charts, the impact of various parameters, including the cross-sectional shape of the column, the grade, and the thickness of the steel, have been examined.



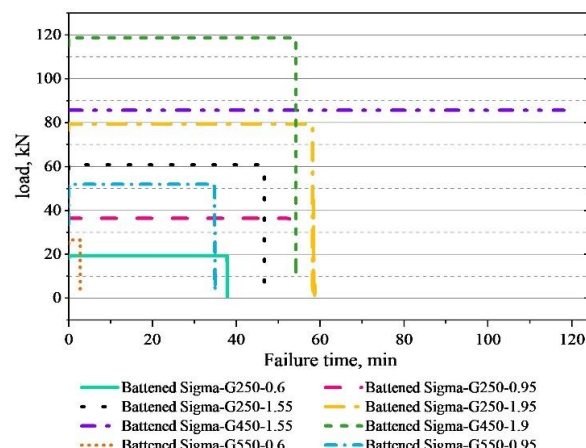
(a)



(b)



(c)



(d)

Fig. 12. Nonlinear numerical results at elevated temperature

#### 4.2.2.1. Effect of Column Cross-Section Shape

Table 5 below presents the statistical analysis of failure times for different column cross-section shapes under fire conditions.

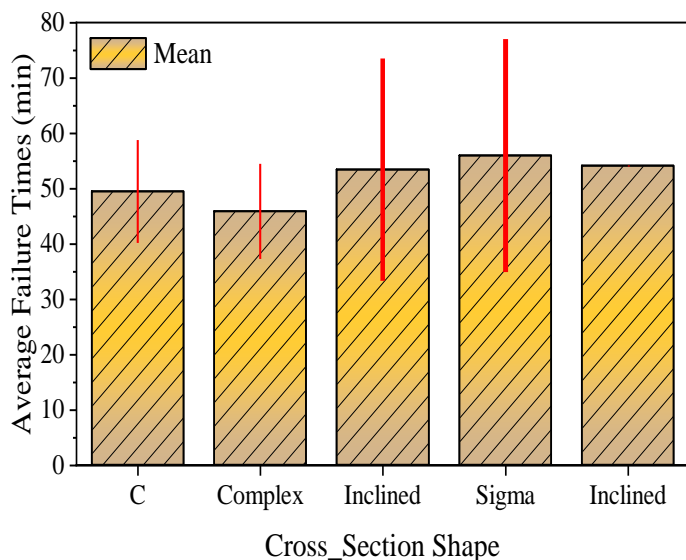


Fig. 13. Effect of Column Cross-Section Shape on ultimate load under fire condition.

Table 5. failure times for different column cross-section shapes under fire conditions.

Cross-Section Shape	mean	std	percentage_diff
C	49.51	9.33	7.89
Complex	45.89	8.13	0
Inclined	53.40	29.04	16.36
Sigma	55.95	26.36	21.94
inclined	54.12		17.93

As can be seen in Fig. 13 the columns with a Sigma cross-section shape have the highest average failure time of 55.96 minutes, indicating better performance under fire conditions. This is 21.94% higher than the Complex shape, which has the lowest mean failure time. Inclined shapes show considerable variation in failure times, with an average of 53.40 minutes and a high standard deviation, reflecting inconsistent performance. The percentage difference from the Complex shape is 16.37%. Columns with a C cross-section have a mean failure time of 49.52 minutes. This represents a 7.90% increase over the Complex shape. Complex shaped has the lowest average failure



time of 45.89 minutes, serving as the baseline for percentage difference calculations. The lowercase "inclined" category also shows a high mean failure time of 54.12 minutes, with a 17.93% increase over the Complex shape. These results indicate that the choice of cross-section shape significantly impacts the fire resistance of columns, with Sigma and Inclined shapes offering better performance compared to Complex shapes.

#### 4.2.2.2. Effect of Column Steel Grade

Table 6 presents the effect of steel grade on average failure time of column under fire condition. Steel Grade 450 exhibits the highest average failure time of 61.46 minutes, indicating the best performance under fire conditions. This is 50.14% higher than Steel Grade 550, which has the lowest mean failure time. Steel Grade 250 shows a moderate average failure time of 51.23 minutes, with a 25.15% increase over Steel Grade 550. Steel Grade 550 has the lowest average failure time of 40.94 minutes, serving as the baseline for percentage difference calculations.

Table 6. failure times of column for different steel grades under fire conditions.

Steel_Grade	mean	std	percentage_diff	median
250	51.23	19.52	25.14	47.48
450	61.45	23.34	50.13	54.14
550	40.93	6.03	0	39.21

Fig. 14 visually represents the effect of different steel grades on the average failure time of columns under fire conditions. Steel Grade 450 exhibits the highest average failure time, indicating the best performance under fire conditions. Steel Grade 250 demonstrates a moderate increase in failure time compared to Steel Grade 550 and Steel Grade 550 Serves as the baseline with the lowest average failure time. The results suggest that columns made from Steel Grade 450 have significantly higher fire resistance compared to those made from Steel Grades 250 and 550. The higher failure time for Steel Grade 450 indicates better performance, making it a preferable choice for fire-resistant column designs.

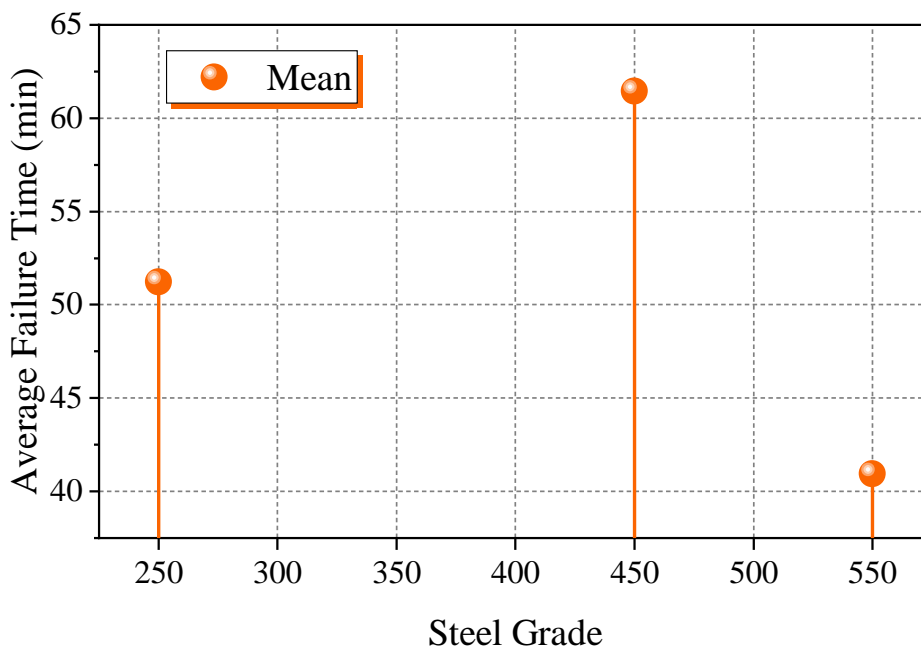


Fig. 14. Effect of Column Steel Grade on ultimate load under fire condition.

#### 4.2.2.3. Effect of Column Steel Grade

Table 7 and Fig.15 presents the statistical analysis of failure times for different steel thicknesses under fire conditions, column with 1.95 mm Steel Thickness exhibits the highest average failure time of 73.49 minutes, indicating the best performance under fire conditions. This is 92.10% higher than the 0.60 mm thickness, which has the lowest mean failure time. Column with 1.55 mm Steel Thickness Shows a considerable

average failure time of 57.28 minutes, with a 49.72% increase over the 0.60 mm thickness. 1.90 mm steel thickness column demonstrates a similar increase in failure time compared to the 1.55 mm thickness, with a mean of 56.73 minutes and a 48.28% increase over the 0.60 mm thickness. Column with 0.95 mm Steel Thickness has a moderate average failure time of 44.22 minutes, with a 15.58% increase over the 0.60 mm thickness. Steel Thickness 0.60 mm serves as the baseline with the lowest average failure time of 38.26 minutes.

Table 7. failure times for different steel thicknesses under fire conditions.

Steel_Thickness	mean	std	percentage_diff
0.6	38.25	3.12	0
0.95	44.21	6.48	15.57
1.55	57.27	24.66	49.72
1.9	56.72	3.07	48.27
1.95	73.48	29.93	92.09

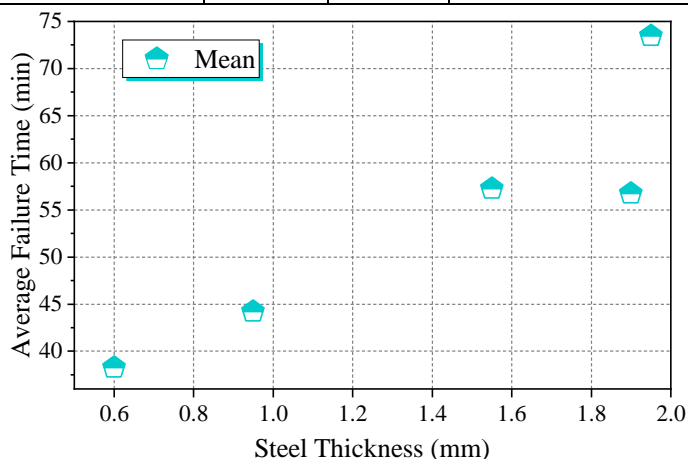


Fig. 15. Effect of Column Steel Grade on ultimate load under fire condition.

To analyze the interaction effects between the parameters on the ultimate load capacity of steel columns, a regression model will be used. An interaction term will be included in the regression model to determine how the combination of different parameters affects the failure time. This approach will capture the synergistic effects between variables such as column cross-section shape, steel grade, and steel thickness. By employing this model, the joint contributions of these parameters to the load-bearing capacity and failure characteristics of steel columns will be quantified, providing a more nuanced understanding of their combined impacts on structural performance.

A regression model will be used to analyze the interaction effects between the parameters. Specifically, an interaction term in the regression model will be employed to examine how the combination of parameters affects the failure time. Fig 16 shows the interaction between steel thickness, steel grade, and failure time, with different colors representing different cross-section shapes. Fig. 16 presents that:

1. **Steel Thickness:** Generally, increasing steel thickness tends to increase the failure time, but the effect is influenced by the cross-section shape and steel grade.

2. **Cross-Section Shape:** Different shapes interact with steel thickness and grade differently, impacting the failure time.
3. **Steel Grade:** The interaction between steel grade and thickness shows that higher grades combined with greater thicknesses tend to increase failure time, though the effect varies by shape.

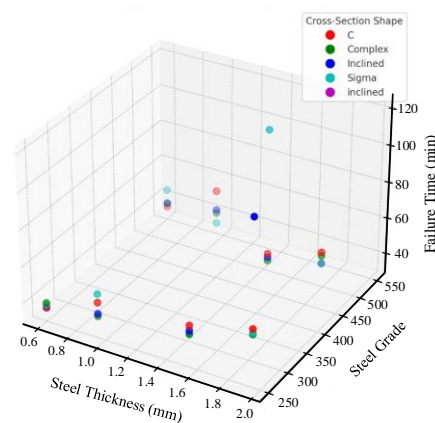


Fig. 16. Statistical Interaction Analysis.

The 3D surface plots shown in Fig. 17 provide a comprehensive view of the interaction between steel thickness, steel grade, and failure time for each cross-section shape. Here are some key observations:

1. **C Shape:**
  - The failure time increases with both steel thickness and grade.
  - Higher steel grades and thicknesses lead to significantly higher failure times.
2. **Complex Shape:**
  - Similar trend to C shape, with failure time increasing with thickness and grade.
  - The interaction between grade and thickness has a noticeable impact on failure time.
3. **Inclined Shape:**
  - Shows a substantial increase in failure time with higher steel thickness, especially for higher grades.
  - The effect of steel grade is more pronounced at higher thicknesses.
4. **Sigma Shape:**
  - Demonstrates a consistent increase in failure time with both steel thickness and grade.

- The overall pattern is similar to the other shapes, but with some variability in the increase rate.

#### 5. inclined Shape:

- Exhibits the highest variability among the

shapes.

- Failure time increases with thickness and grade, but the rate of increase is less consistent compared to other shapes.

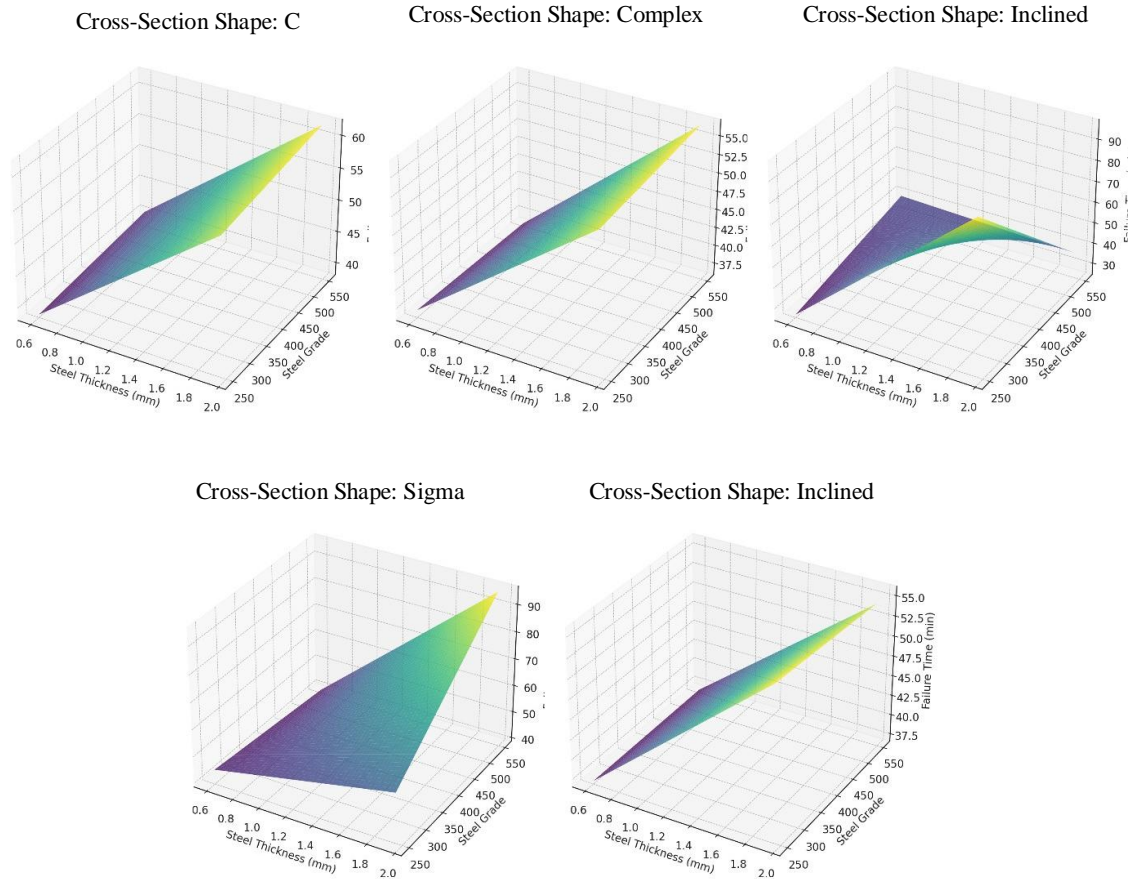
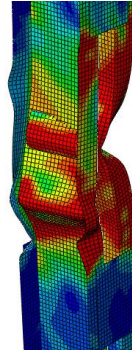
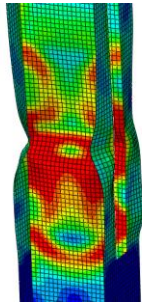


Fig. 17. interaction between steel thickness, steel grade, and failure time for each cross-section shape.

#### 4.2.3. Failure modes

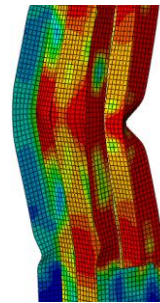
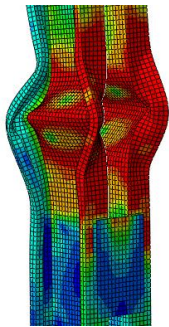
Fig. 18 shows the failure modes of cold-formed columns with different cross-section shapes, steel grades, and thicknesses under fire conditions. The failure modes of CFS columns under fire conditions are influenced by cross-sectional shape, steel grade, and thickness. Sigma-shaped columns tend to exhibit local buckling in their web and flange areas, exacerbated by thermal gradients causing uneven deformation. Inclined columns experience combined bending and buckling, with fire conditions intensifying these modes due to the inclination causing twisting. Complex-shaped columns show significant local and distortional buckling, with the intricate geometry leading to asymmetric heat distribution and uneven failure. In contrast, C-shaped columns primarily undergo flexural and local buckling, where the open section design leads to rapid heat

transfer and flange deformation. Steel grade plays a crucial role: lower grade G250 steel softens more quickly under heat, leading to pronounced buckling and early failure, while higher grade G550 steel, although initially more resistant, eventually loses strength, causing delayed but potentially more sudden failure due to higher residual stresses. The thickness of the steel also affects performance; thinner sections (0.6 mm) heat up faster and lose strength quickly, resulting in early local buckling, while thicker sections (1.95 mm) heat more slowly, offering better initial resistance but succumbing to buckling under extended fire exposure. This analysis reveals that while thicker, higher-grade steel columns offer better initial resistance to fire, complex cross-sectional shapes and thin sections are more vulnerable to rapid failure due to uneven heating and rapid strength degradation.



**C-G250-0.6**

**C-G250-1.95**



**Co-G250-1.95**

**S-G250-1.95**

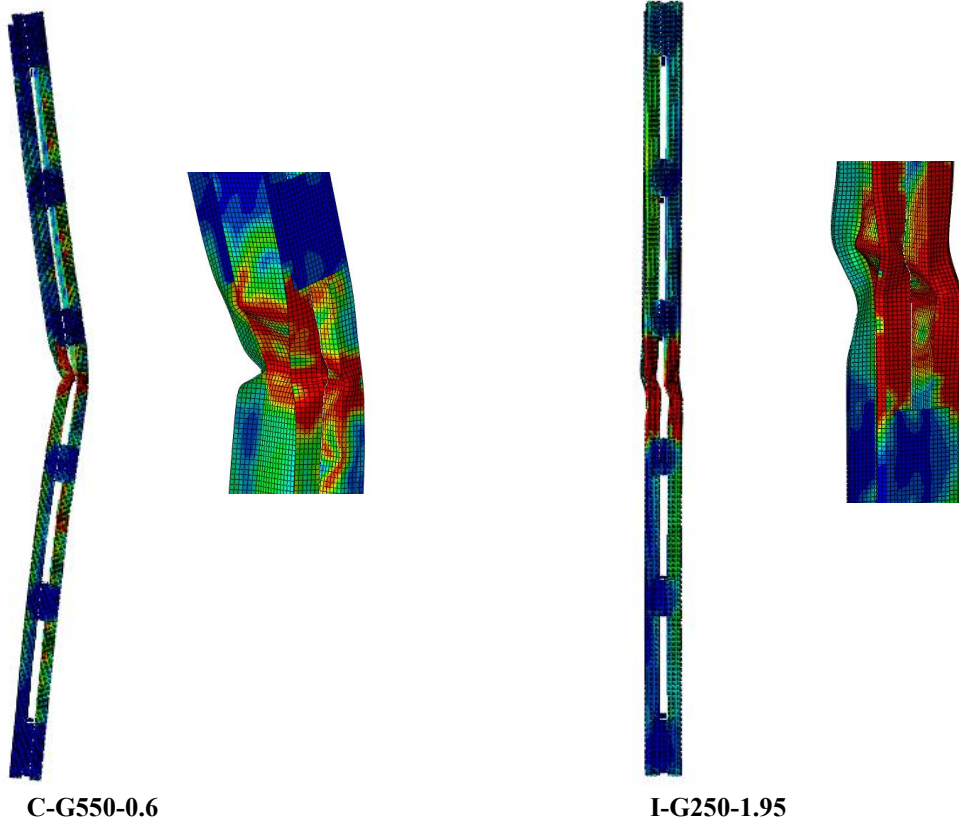


Fig. 18. Failure modes of columns.

## 5. Conclusion

This study offers a comprehensive examination of the ultimate load capacity of steel columns by analyzing the effects of column cross-section shape, steel grade, and steel thickness. The findings provide crucial insights into optimizing structural design for enhanced load-bearing performance. The results at ambient temperature shows that:

- **Cross-Section Shape:** The Complex shape exhibited the highest load capacity (178.51 kN), outperforming other configurations, with the Inclined shape showing notable variability and reaching up to 237.68 kN. The Sigma and Inclined shapes provided intermediate load capacities, highlighting the significant role of geometric configuration in maximizing column strength.
- **Steel Grade:** G450 steel demonstrated superior performance with an average load capacity of 195.01 kN, nearly double that of G250 (99.55 kN), while G550 showed reduced load capacity (93.09 kN), likely due to brittleness. This indicates G450 as the optimal grade for balancing strength and ductility.
- **Steel Thickness:** Increasing thickness generally

enhanced load capacity, with an optimal point at 1.90 mm (209.15 kN), after which performance declined. This suggests that further increases in thickness may not proportionally enhance capacity.

### At Elevated Temperatures:

- **Steel Thickness:** Thicker columns improved fire resistance, with 1.95 mm steel providing the highest failure time (73.49 minutes), significantly outperforming thinner steel (0.60 mm at 38.26 minutes).
- **Steel Grade:** G450 steel offered the highest fire resistance, with a failure time of 61.46 minutes, outperforming G250 and G550 by 25.15% and 50.14%, respectively.
- **Cross-Section Shape:** Sigma and Inclined shapes showed the highest fire resistance, with failure times of 55.96 and 53.40 minutes, respectively, compared to the Complex shape at 45.89 minutes.
- **Interaction Effects:** Complex interactions between thickness, grade, and shape significantly influenced performance, as confirmed by the ANOVA test ( $p$ -value = 0.014). Thicker and higher-grade steels generally improved fire resistance, but the extent



varied by cross-sectional shape.

These findings provide valuable guidelines for optimizing the design of steel columns to improve structural efficiency and fire resistance, contributing to safer and more cost-effective construction practices.

Based on the findings of this study, it is recommended that future fire design codes incorporate specific provisions for built-up cold-formed steel (CFS) columns, with attention given to the role of batten plates, the optimization of cross-sectional

shapes such as Complex and Sigma, and the selection of appropriate steel grades and thicknesses for enhanced fire resistance. Additionally, it is suggested that standardized fire resistance testing be expanded to include built-up columns with varied geometries, and that non-uniform temperature distribution during fire exposure be accounted for to improve the accuracy of fire performance predictions. These recommendations are intended to enhance the structural safety and fire resilience of CFS columns in building designs.

## References

1. Rathore, K., Gupta, M. K., & Verma, M. (2023). A comprehensive review on cold-formed steel building components. *Recent Trends in Mechanical Engineering: Select Proceedings of PRIME 2021*, 461–468. [https://doi.org/10.1007/978-981-19-7709-1\\_46](https://doi.org/10.1007/978-981-19-7709-1_46)
2. Dai, Y., Roy, K., Fang, Z., Raftery, G. M., Ghosh, K., & Lim, J. B. (2023). A critical review of cold-formed built-up members: Developments, challenges, and future directions. *Journal of Building Engineering*, 64, 107255.
3. Kopecki, T., & Mazurek, P. (2014). Numerical representation of post-critical deformations in the processes of determining stress distributions in closed multi-segment thin-walled aircraft load-bearing structures. *Eksploatacja i Niezawodność – Maintenance and Reliability*, 16(1), 163–169.
4. Chen, M. T., Pandey, M., & Young, B. (2021). Mechanical properties of cold-formed steel semi-oval hollow sections after exposure to ISO-834 fire. *Thin-Walled Structures*, 167, 108202.
5. Zuo, W., Chen, M. T., & Young, B. (2024). Structural behaviour of cold-formed steel elliptical hollow section stub columns after exposure to ISO-834 fire curve. *Thin-Walled Structures*, 197, 111309.
6. Chen, M. T., Pandey, M., & Young, B. (2021). Post-fire residual material properties of cold-formed steel elliptical hollow sections. *Journal of Constructional Steel Research*, 183, 106723.
7. Li, Q. Y., & Young, B. (2023). Experimental and numerical studies on cold-formed steel battened columns. *Engineering Structures*, 288, 116110.
8. Yin, L., Li, R., Wang, X., Chen, W., Ye, J., & Wu, X. (2024). Fire experiments on cold-formed steel square tubular columns with new gypsum sheathing configuration. *Thin-Walled Structures*, 197, 111727.
9. Kotelko, M., Macdonald, M., Kulatunga, M. P., & Marszalek, Z. (2020). Upper-bound estimation of load-carrying capacity of perforated cold-formed thin-walled steel lipped channel columns under compression loading. *Eksploatacja i Niezawodność – Maintenance and Reliability*, 22(3), 565–573. <https://doi.org/10.17531/ein.2020.3.20>
10. Dębski, H. (2013). Experimental investigation of post-buckling behavior of composite column with top-hat cross-section. *Eksploatacja i Niezawodność – Maintenance and Reliability*, 15(2), 106–110.
11. Yang, J., Wang, W., Xu, L., & Shi, Y. (2023). Global buckling analysis on cold-formed steel built-up box-shape columns at ambient and elevated temperatures. *Structures*, 57, 105301.
12. Yang, J., Zhou, X., Wang, W., Xu, L., & Shi, Y. (2023). Fire resistance of box-shape cold-formed steel built-up columns failing in global buckling: Test, simulation and design. *Thin-Walled Structures*, 183, 110433.
13. Sabu Sam, V., Adarsh, M. S., Lyngdoh, G. R., Marak, G. W. K., Anand, N., Al-Jabri, K., & Andrushia, D. (2023). Influence of elevated temperature on buckling capacity of mild steel-based cold-formed steel column sections: Experimental investigation and finite element modelling. *Journal of Structural Fire Engineering*, 14(3), 487–504. <https://doi.org/10.1108/JSFE-08-2023-0033>
14. Pires, T. A., do Rêgo Silva, J. J., dos Santos, M. M., & Costa, L. M. (2021). Fire resistance of built-up cold-formed steel columns. *Journal of Constructional Steel Research*, 177, 106456.
15. Chen, M. T., Pandey, M., & Young, B. (2021). Post-fire residual material properties of cold-formed steel elliptical hollow sections. *Journal of Constructional Steel Research*, 183, 106723.
16. Yang, J., Wang, W., Shi, Y., & Xu, L. (2020). Experimental study on fire resistance of cold-formed steel built-up box columns. *Thin-Walled*

Structures, 147, 106564.

17. Yang, J., Shi, Y., Wang, W., Xu, L., & Al-azzani, H. (2020). Experimental and numerical studies on axially restrained cold-formed steel built-up box columns at elevated temperatures. *Journal of Constructional Steel Research*, 171, 106143.
18. Muftah, F., Sani, M. S. H. M., Osman, A. R., Mohammad, S., & Ngian, S. P. (2018). Experimental investigation on box-up cold-formed steel columns in fire. *GEOMATE Journal*, 14(44), 58–64. <https://doi.org/10.21660/2018.44.3538>
19. Eurocode 3: Design of steel structures. Part 1-3: Design of cold-formed steel structures. ECCS – European Convention for Constructional Steelwork, Wiley-Blackwell, 676 p.
20. Craveiro, H. D., Rodrigues, J. P. C., & Laím, L. (2016). Experimental analysis of built-up closed cold-formed steel columns with restrained thermal elongation under fire conditions. *Thin-Walled Structures*, 107, 564–579. <https://doi.org/10.1016/j.tws.2016.07.001>
21. Rodrigues, J. P. C. (2015). Built-up closed cold-formed steel columns with restrained thermal elongation subjected to fire. *Response of Structures Under Extreme Loading (PROTECT 2015)*.
22. Batista Abreu, J. C., Vieira, L. M., Abu-Hamd, M. H., & Schafer, B. W. (2014). Development of performance-based fire design for cold-formed steel. *Fire Science Reviews*, 3, 1–15. <https://doi.org/10.1186/s40038-014-0001-3>
23. Craveiro, H. D., Rodrigues, J. P., & Laím, L. (2013). Baseline study on the behaviour of cold-formed steel columns subjected to fire. *Applications of Structural Fire Engineering*.
24. ABAQUS Standard User's Manual. (2008). Version 6.8, Dassault Systèmes Simulia Corp., Providence, RI, USA.
25. Dębski, H., Koszałka, G., & Ferdynus, M. (2012). Application of FEM in the analysis of the structure of a trailer supporting frame with variable operation parameters. *Eksplatacja i Niezawodność – Maintenance and Reliability*, 14(2), 107–114.
26. Falkowicz, K., Ferdynus, M., & Dębski, H. (2015). Numerical analysis of compressed plates with a cut-out operating in the geometrically nonlinear range. *Eksplatacja i Niezawodność – Maintenance and Reliability*, 17(2), 222–227. <https://doi.org/10.17531/ein.2015.2.8>
27. ISO 834-1. (1999). Fire resistance tests – Elements of building construction, Part 1: General requirements. International Organization for Standardization, Geneva, Switzerland.
28. Dias, Y., Keerthan, P., & Mahendran, M. (2018). Predicting the fire performance of LSF walls made of web stiffened channel sections. *Engineering Structures*, 168, 320–332. <https://doi.org/10.1016/j.engstruct.2018.04.072>
29. Craveiro, H. D. S. (2015). Fire resistance of cold-formed steel columns (Ph.D. thesis). University of Coimbra, Portugal.
30. Ramzy, K. (2014). Effect of batten plates on the behaviour and strength of cold-formed steel built-up section columns. (Master's thesis). Tanta University, Tanta, Egypt.
31. Dabaon, M., Ellobody, E., & Ramzy, K. (2015). New tests on built-up cold-formed steel section battened columns. In *ICASGE '15, International Conference on Advances in Structural and Geotechnical Engineering*, Hurghada, Egypt, 6–9 April. <https://doi.org/10.1016/j.tws.2015.03.001>
32. Dabaon, M., Ellobody, E., & Ramzy, K. (2015). Experimental investigation of built-up cold-formed steel section battened columns. *Thin-Walled Structures*, 92, 137–145. <https://doi.org/10.1016/j.tws.2015.03.001>
33. Ellobody, E., & Young, B. (2005). Behaviour of cold-formed steel plain angle columns. *Journal of Structural Engineering ASCE*, 131(3), 457–466. [https://doi.org/10.1061/\(ASCE\)0733-9445\(2005\)131:3\(457\)](https://doi.org/10.1061/(ASCE)0733-9445(2005)131:3(457))
34. Senthilkumar, R., & Kumar, D. P. (2021). Numerical studies on restrained cold-formed steel column subjected to transient thermal loading. *Structures*, 34, 712–724. <https://doi.org/10.1016/j.istruc.2021.03.030>
35. Kankanamge, N. D., & Mahendran, M. (2011). Mechanical properties of cold-formed steels at elevated temperatures. *Thin-Walled Structures*, 49, 26–44. <https://doi.org/10.1016/j.tws.2010.08.004>
36. Ranawaka, T., & Mahendran, M. (2009). Experimental study of the mechanical properties of light gauge cold-formed steels at elevated temperatures. *Fire Safety Journal*, 44, 219–229. <https://doi.org/10.1016/j.firesaf.2008.06.006>

### Acronyms

CFS	Cold-formed steel
CFSEHS	Cold-formed steel elliptical hollow sections
C	Lipped channel section



2D	Two dimensional
3D	Three dimensional
FEA	Finite element analysis
FEM	Finite element method
FRR	Fire resistance rating
ISO	International organization for standardization
MPC	Multiple point constraint
$P_i$	Axial applied force
R	Axial restraining force
RP	Reference point
$\sigma_{true}$	True stress
$\sigma_{nom}$	Nominal stress
$\varepsilon_{nom}$	Nominal strain
$\varepsilon_{in}^{pl}$	Plastic strain
$E$	Elastic modulus